Rivulet Flows in Microchannels and Minichannels

Kabov O.A.[1,2,3,4], Bartashevich M.V.[1,2] and Cheverda V.[1,3,*]
[1]Heat Transfer International Research Institute of Universite Libre de Bruxelles and Institute of Thermophysics RAS, Brussels, Belgium
[2]Institute of Thermophysics, Russian Academy of Sciences, prosp. Lavrentyev 1, Novosibirsk, 630090 Russia
[3]Universite Libre de Bruxelles, Chimie-Physique EP-CP165/62, Microgravity Research Center, Avenue F.D.Roosevelt 50, Bruxelles, B-1050, Belgium
[4]Center of Smart Interfaces, Technische Universität Darmstadt, Petersen str. 32, 64287 Darmstadt, Germany

ABSTRACT

Thin liquid films or rivulets may provide very high heat transfer intensity, especially in the micro region near contact-line and may be used for cooling of microelectronic equipment or engines. The paper focuses on the recent progress that has been achieved in the understanding of the rivulet flow phenomena in micro/mini-channels through conducting experiments and theory. Experiments on a gas shear-driven rivulet flow in a minichannel have been done during four parabolic flights campaigns of the European Space Agency. The phase shift schlieren technique and a conventional schlieren technique have been used for two-phase flow visualization. The force balance is varied during a parabolic flight and due to surface tension effect the liquid film in a minichannel 40 mm width became a flattened rivulet 9 mm width at microgravity. The rivulet reaches the certain equilibrium width at microgravity. The numerical calculations of the flow depending on the gravity forces have been made. It was found also that the rivulet width and shape is changing with gravity. The character of shear- and gravity driven rivulet flowing is different at horizontal micro- and minichannels. The comparison of numerical and analytical results with experimental data has been carried out.

Keywords: Liquid rivulet, gas flow, minichannel, surface tension, thin liquid film, gravity effect, parabolic flights.

Nomenclature

a	[m]	source diameter
b	[m]	semi width of rivulet
d	[m]	minichannel height
f	[m]	focal length of the Schlieren lens
g_0	[m/s^2]	normal gravitational acceleration
g	[m/s^2]	gravitational acceleration
$H(y)$	[m]	profile of rivulet in (y, z)- plane
q	[m^{-1}]	inverse of capillary length $q = (\rho g/\sigma)^{1/2}$
Q	[m^3/s]	flow rate
l	[m]	channel width
Re	[-]	Reynolds number, $\mathrm{Re} = Q\rho/\mu l$
v	[m/s]	liquid velocity in rivulet
y	[m]	Cartesian axis direction, horizontal
z	[m]	Cartesian axis direction, perpendicular to the plane

*Author for correspondence, E-mail: vcheverd@ulb.ac.be

Special Characters

α	[radian]	surface slope
α_Λ	[radian]	range of angle deviation
β	[radian]	channel inclination angle
θ	[radian]	contact angle
μ	[kg/ms]	dynamic viscosity
ν	[m^2/s]	kinematic viscosity
ρ	[kg m^{-3}]	density
σ	[N/m]	surface tension coefficient
τ	[kg/ms^2]	tangential gas shear-stress on the gas-liquid interface
Λ	[m]	Schlieren filter period
Ω	[m^2]	rivulet cross section

Subscripts

g	gas
l	liquid or without subscript

1. INTRODUCTION

A rivulet flowing at mini- and microchannels, as a special case of two-phase flows, can be very promising in earth and space applications: microelectronic cooling devices, heat exchangers (enhancement of heat transfer due to their two contact areas), life support systems and waste water treatment for long duration space exploration missions, microfluidics. The shear-driven rivulet flows have significant peculiarities in conditions of low gravity. Also behaviour of rivulets differs for micro- and minichannels. The understanding of the fundamental aspects of the rivulet dynamics provides a way to control such flows.

In numerous works devoted to the study of rivulet flow, the surface of rivulet is considered as free [1, 2, 3]. Towell and Rothfeld [1] have considered the equations which describe the hydrodynamics of laminar flow of a liquid rivulet down an inclined surface. Steady state solutions have been obtained for the case of no shear stress at the liquid- gas boundary and relate the flow rate to the rivulet width, the physical properties of the liquid, and the contact angle. At some following works rivulet geometry, rivulet stability and transition to meander flow have been investigated. Bentwich et al. [3] has developed an analytical solution for the velocity distribution of rectilinear rivulet flow down a vertical plate. The polynomial solution for the case of an inclined plate was obtained by generalized Ritz-Galerkin method. Allen and Biggin [2] presented the theoretical analysis of the velocity distribution within a lenticular liquid filament flowing down an inclined plane. The external gas phase was assumed to have no effect; surface tension and contact angle were taken to be constant. The solution based on a series expansion whose validity depends on the smallness of the filament's height to width ratio was compared graphically with an exact numerical solution. The gas-liquid lenticular interface was determined in such a way that all constants are known directly in terms of measurable physical parameters.

Schmuki and Laso [4] investigated the effects of the flow rate, viscosity, surface tension, and showed that meandering is suppressed at high viscosities. A flow regimes classification has been suggested. Alekseenko et al. [5] presented the mathematical model of rivulet flowing down on the inclined cylinder in the absence of external shear stress on the free surface. The velocity vector is parallel to the axis of the cylinder. The flow is laminar and steady. Rivulet profile and velocity do not vary downstream. Also, the complete family of curves describing the free rivulet surface was found taking into account the surface tension and specification of the contact angle value. The relations of the main geometric parameters of the rivulet (cross-sectional area, semi-width, height) from the liquid flow rate have been obtained. The velocity field has been calculated on the basis of solutions of two-dimensional Poisson equation in the rivulet profile by the boundary integral equations method.

Perazzo and Gratton [6] have provided an analytic formula of the shape of the free surface, which was obtained by solving the equation that expressed the condition of static equilibrium under the action of gravity and surface tension. The velocity field was obtained by solving a Poisson equation in the domain defined by the cross-section of the rivulet. The analytic solution for the shape of the free surface near contact line was presented.

At all mentioned models of rectilinear rivulet the shear-stress effect of gas phase on a free surface has not been investigated. Also the contact angle has been considered invariable. That is, the influence of the dynamic characteristics of gas flow on the fluid motion is neglected. The question of finding the velocity field in the gas did not arouse. However, such free surfaces are only a special case of a more general concept of the interfacial boundaries, which must take into account the dynamic effects of gas flow on the fluid flow and phase transformations.

Some experimental results for wavy rivulet flowing down an inclined tube were presented by Alekseenko et al. [7, 8, 9]. In [7] it was shown that the rivulet flow is unstable and nonlinear wavy regimes may be developed. In [8] the analysis of liquid velocity fields inside the hump of the developed stationary waves was made using the PIV technique. It was found that the vortex motion exists in the hump. In [10] the wavy rivulets flowing down a vertical plate have been investigated using Laser Induced Fluorescence method (LIF). The wave structure of rivulets for different wave regimes and Reynolds numbers was obtained. It was found that general property of rivulet flow is insensitivity of contact angles of rivulets to the wavy motion at all contact angles. Nevertheless, it was found that the wave structure of rivulets is sufficiently different for small and large contact angles. Gambaryan-Roisman and Stephan [11] was presented the investigation of the stability characteristics of rivulets on walls with topography under the simultaneous action of gravity and thermocapillarity.

Thermocapillary convection in a liquid film gravitationally-falling down locally heated substrate has been studied in [12]. It was shown that due to intensive local heating the liquid film can break spontaneously into a jets and a thin film between them. This thin film evaporates intensely and a system of parallel rivulets forms. Some experimental, theoretical and numerical results are performed in [13]. The system of parallel flowing rivulets of the liquid FC-72 has been investigated in [14]. The jet formation at presence of two-dimensional and three-dimensional waves in a heated liquid film flowing down a vertical surface was studied in [15].

The cause of formation of parallel flowing rivulets can be not only the thermocapillary forces. Pavlenko and Lel in [16, 17] investigated the development of jets of cryogenic liquid in falling films down a heated vertical surface. The intensive boiling and evaporation in the liquid film leads to the formation of rivulet-similar structures.

Myers et.al. [18] replaced the gas flow action on the fluid by the presence at the interface the constant shear stress directed along the axis. Bartashevich et al. [19, 20] and Kabov et al. [21] have investigated the fully-developed rivulet and gas flow in minichannels in conditions of variable gravity. This two-phase flow regime was investigated experimentally and numerically for linear straight rivulet flows at microgravity and earth gravity conditions. The mathematical model describes steady-state isothermal rivulet and gas flow with the constant cross section. The rivulet profile is a result of the tangential, gravity and capillary forces. The geometry of rivulet profile is described by the static (equilibrium) contact angle between the fluid and the solid surface. The experimental results were compared with numerical results for laminar rivulet. However, especially in microchannels, there is no possibility to use such the constant shear stress simplification [22].

Investigations on isothermal and non-isothermal rivulets flow are extremely important for the future systems with intensive heat and mass transfer, with high heat flux density and height heat flux volumetric intensity. Some examples can be: power plant steam generators; nuclear-heated rod bundles; 3-D microelectronics and modern power electronics in cars, trains, ships, aircrafts and spaceship. The main motivation of the rivulet using is the theoretical possibility of significant enhancement of heat transfer. The rivulets may occur spontaneously or can be specially created.

The investigation of the influence of co-current gas flow on the rivulet dynamics is one of the important aspects of systematic investigations on physics of rivulets. The present review paper focuses on the recent progress that has been achieved in the understanding of the rivulet flow phenomena in micro/mini-channels through conducting experiments and theory. Nevertheless, an important amount of new results has been also presented. The paper is organized as follows. In the following sections, after the nomenclature, the apparatus for experimental investigations in laboratory and parabolic flights of aircraft conditions as well as optical measurement techniques are discussed. In section 5, experimental results both for normal gravity and microgravity conditions are presented. Analytical model and numerical results are described in section 6. In section 7, comparison of theoretical and experimental results is discussed. We conclude in section 8.

2. EXPERIMENTAL APPARATUS AND MEASURIMENT TECHNIQUE

2.1. Experimental Setup for On-Ground Experiments

Figure 1 shows a photograph of experimental setup. The test section design is shown in Fig. 2. Dialectical liquid FC-72 and nitrogen were used as working liquid and gas, respectively. Temperature of the heated substrate as well as inlet and outlet temperatures of gas and liquid has been measured with K-type thermocouples with precision of about 0.2 °C. Five thermocouples on the substrate are placed from the liquid nozzle at the distances: 5, 20, 35, 50 and 65 mm, respectively.

Hydraulic schematic of the experimental apparatus consists of: 1) gas supply system; 2) liquid supply system; 3) Vapor-gas pumpdown system and 4) water cooling system. Nitrogen gas is supplied from a balloon. Working pressure and gas flow rate are regulated automatically through a computer by pressure control and measurement and by flow control and measurements gauges. Nitrogen gas flow rate is varied from 10 ml/minute to 50 l/minute with an uncertainty less than 3% using two different gauges mounted in parallel. Pressure rate is varied from 0.8 to 1.2 bar also using two different gauges mounted in parallel.

Controlled by syringe pump the working liquid FC-72 is supplied from liquid container into a buffer chamber of test section. The liquid flow rate has been varied in the range 1–30 ml/min and has been measured with the uncertainty less than 1%. The film, formed in the nozzle of variable height (50–100 μm),

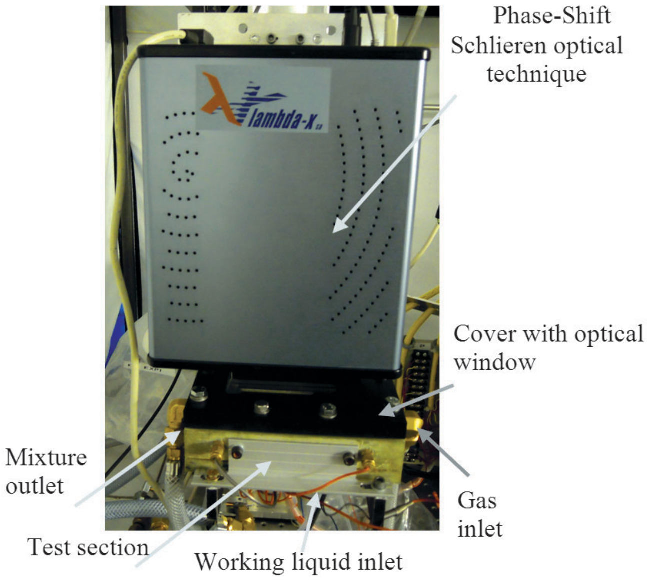

Figure 1. Photograph of experimental setup.

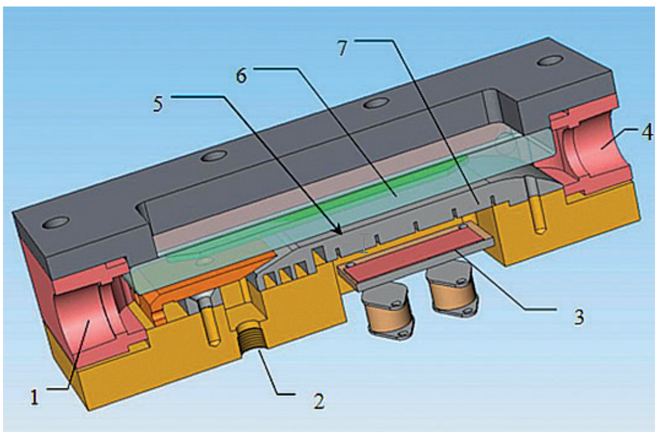

Figure 2. Experimental test section: 1 – gas inlet, 2 – liquid inlet, 3 – electric heater, 4 – outlet, 5 – channel, 6 – transparent cover, 7 – heated substrate.

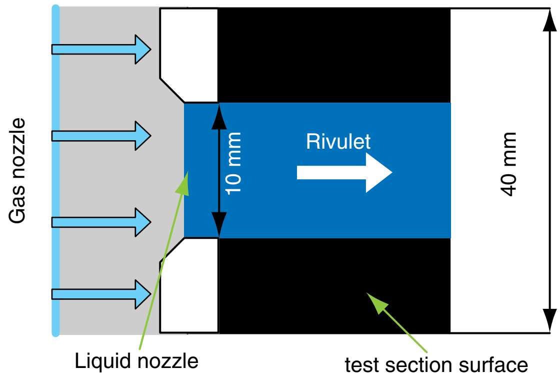

Figure 3. Concept of the nozzle for creation of the rivulet flow.

is driven along the channel by the moving gas. The gas and residual apour has been evacuated to the atmosphere by vacuum pump. Diaphragm vacuum pump is used to provide necessary depression at the outlet of the test sections in the case of relatively large gas flow rate. It also allows performing of the tests at low working pressure. Cooling system is based on the use of thermo-electrical modules (Peltier elements). The system provides chilled purified water of constant temperature in the range of 18…30°C, which is used for equalizing temperature of the gas and the liquid at the inlets to the test section.

The present setup is used for experiments with both: liquid films and rivulets. We consider the rivulet flow as a particular case of film flow when the film occupies only a part of the substrate without touching to the lateral walls of the test section. The rivulet flow has been realized in the channel with blocking part of the liquid nozzle (see Fig. 3).

2.2. Optical System

The "Nimo" – Phase-Shift Schlieren optical technique (PSS) is used for visualisation and measurements of the 3D deformations on the surface of rivulet, of the shape of rivulet and the width of rivulet. It allows measuring the angles of deviation of the light beam after its reflection from the mirror surface of the substrate. The shape of the film can be deduced after the numerical integration of the measured angles along the curvilinear surface [23]. The heated substrate has been coated by a thin film of aluminium with unevenness of ± 1µm and roughness Ra = 0.03. It has a mirror quality.

Field of view of the optical system has been positioned as shown in Fig. 4. The equipment has been supplied as a ready-for-use device (Lambda-X s.a., Belgium) and is shown in Fig. 5. Being applied for the 3D measurements of the film thickness the PSS system allows measurements at

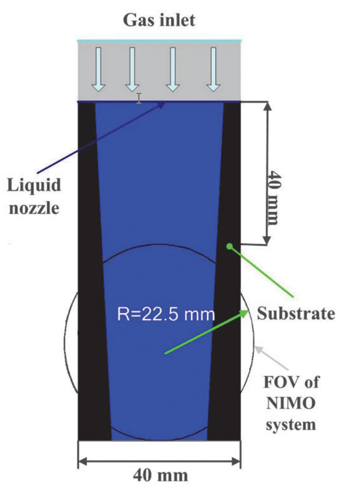

Figure 4. Field of view of the PSS optical system.

Figure 5. Photograph of the PSS optical system.

frequency of 0.3…0.7 Hz. Besides, being used in the Conventional Schlieren mode, the system allows visualization of deformations on the film surface in two perpendicular directions (streamwise or spanwise) at the frame frequency of up to 15 Hz. More details and principal about Schlieren systems operation can be found in [24, 25].

In the conventional Toëpler Schlieren, a knife edge is used as a filter (Fig. 6a) and a typical curve of the intensity reaching the CCD camera as a function of the light beam deviation α is given in Fig. 6b [23, 24].

In the Phase-Shifting Schlieren the filter represents a multi-line element of the sinusoidal transmission (Fig. 7 a). By an adequate choice of the filter period and the source slit width, one arranges the Schlieren system in such a way that the light beam angle deviation is coded over a wide range of the angle by a sinusoidal function (Fig. 7 b). Thus, the capability of the arrangement to generate fringes is called *Schlieren fringes*. Automatically, every fringe corresponds to a range of angle deviation α_Λ that depends on the Schlieren filter period Λ and the focal length *f* of the Schlieren lens:

$$\tan(\alpha_\Lambda) = \frac{\Lambda}{f_2} \tag{1}$$

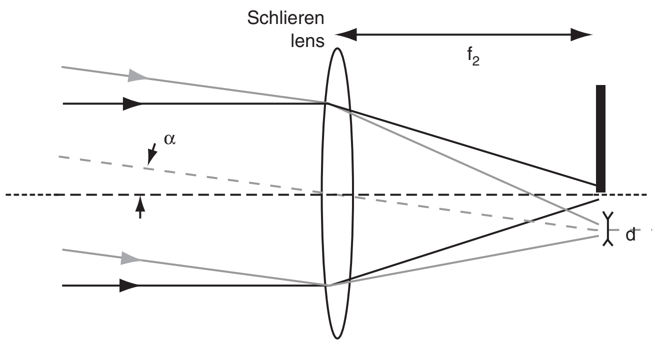

(a) Arrangement of knife edge

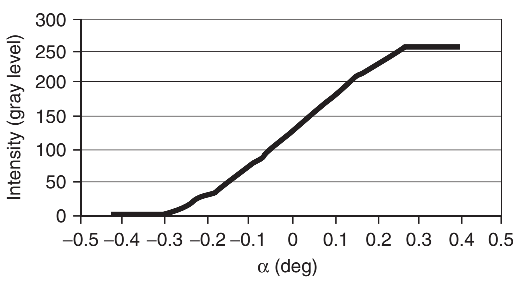

(b) Typical response curve

Figure 6. Conventional Schlieren (a): arrangement of knife edge; (b): typical response curve, [23].

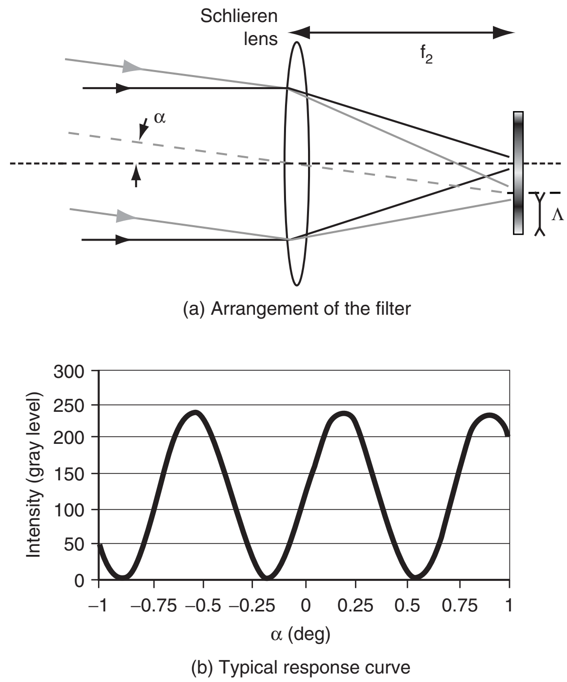

Figure 7. Phase-Shift Schlieren (a): arrangement of the filter; (b): typical response curve, [23].

The angle α_Λ is independent of the extension of the source. The latter will influence only on the visibility and on the shape of the fringes. Total range of the measured deviation angles is limited by sizes of the optical elements only.

It is possible to use measurement option with different frequencies (number of pictures). Precision of measurements rises with the number of images but the duration of the measurements increases as well. The test measurements have been carried out by the algorithms of 3, 5, 10 images consequently. It was defined that the system can provide the frequency of 0.7 Hz for the 3-image algorithm, 0.5 Hz – for 5 images and 0.3 Hz – for 10 images. Figure 8a shows the measured 3-D profile of the concave mirror. Comparison of calibration measurements with the actual profile is shown in Fig. 8b along with the results for the flat mirror. The 2-D profiles have been obtained as cross sections of the 3-D profiles. While the measurement uncertainty for the full field of view (FOV) of 30 mm comes to 2 μm, for the FOV reduced to 20 mm it equals to 1 μm. The advantage of the 3-image algorithm over the 10-image one in the duration of measurements (faster by a factor 2.5) is much more important than the loss of the accuracy of about 0.5 μm. Eventually the 3-image algorithm at the FOV of 20 mm was applied for the experiments. The measurement uncertainty is supposed to be of 1 μm.

2.3. Experimental Setup for Microgravity Experiments

On-ground experimental setup has been modified for microgravity experiments. Parabolic flight experiments have been done during parabolic flights campaigns of the European Space Agency (41st, 44th, 47th and 49th ESA campaigns). Different tests during 372 parabolas have been performed. About 180 parabolas have been dedicated to a rivulet flow investigations in the isothermal conditions.

Aircraft parabolic flights are a useful tool for performing short duration scientific and technological experiments in reduced gravity [26, 27]. The Airbus A300 “Zero G” managed by the Franch company Novespace (subsidiary of the CNES, Franch Space Agency) has been used. The main advantages of parabolic flights for microgravity investigations are: the possibility of modifying the experiment set-up between flights and the possibility of direct intervention by investigators on board the aircraft between parabolas.

During the parabolic flight maneuver gravity levels are changed repetitively, giving successive periods of about 20–22 s of microgravity preceded and followed by periods of 20 s of hypergravity (accelerations up to 1.8–2g_0), Fig. 9. In the reduced gravity period all aircraft engines thrust is strongly reduced, compensating the effect of air drag (parabolic free fall). During the microgravity, the residual

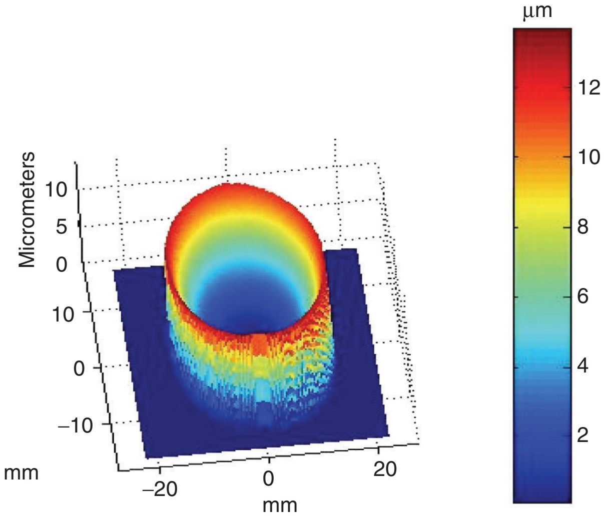

(a) The measured 3-D profile for the concave mirror

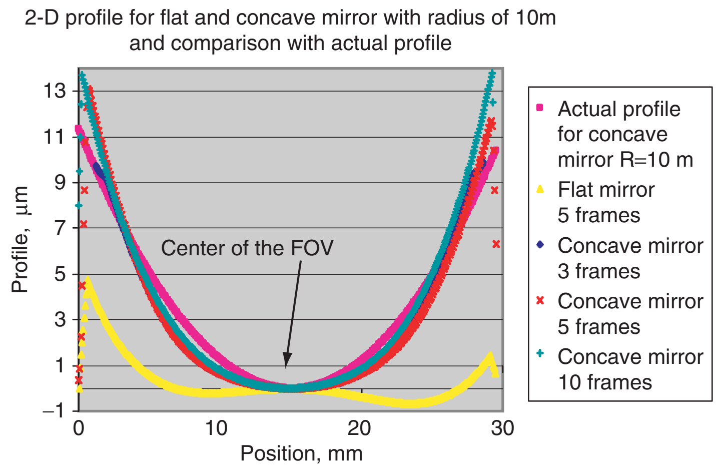

(b) The measured 2-D profiles of the flat and the concave mirrors

Figure 8. Comparison of measured profiles by Phase-Shift Schlieren optical technique with the actual profiles for different algorithms.

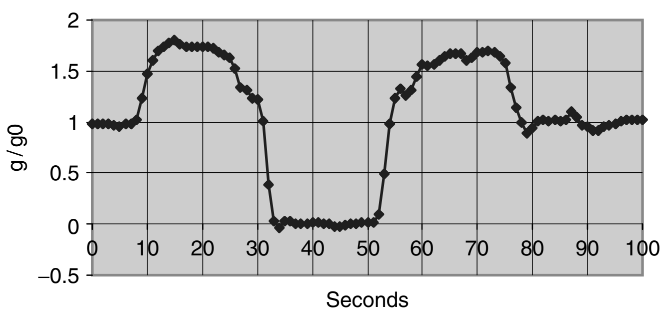

Figure 9. Variation of acceleration during the aircraft maneuver in the direction perpendicular to the flow direction, parabola # 1 on 18.12.2007 (data provided by Novespace).

accelerations measured by sensors attached to the aircraft floor structure are typically in the order of 10^{-2} g_0. A typical duration of one flight is about 2 hours and 30 minutes, allowing for 31 parabolas to be flown, in sets of 5–6 with 2 minutes intervals between parabolas and with 4–6 minutes between sets of parabolas. A typical duration of one campaign is 3 flights days.

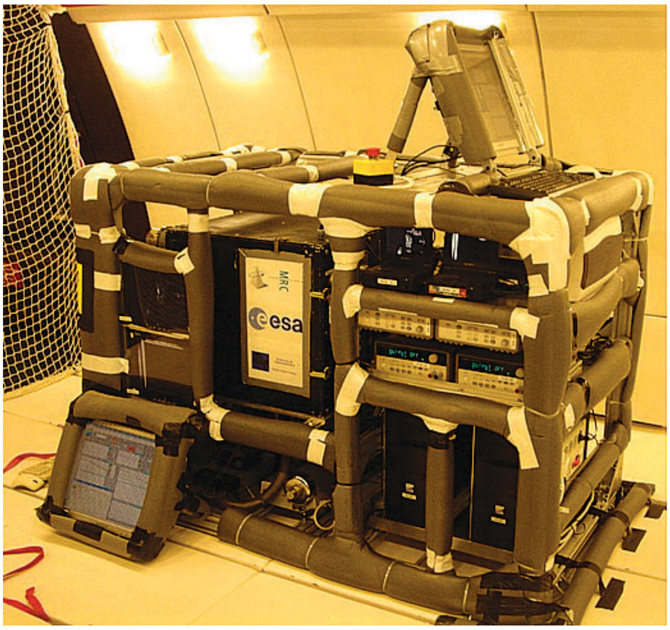

Figure 10**.** Photograph of experimental setup onboard the aircraft during the parabolic flights experiments, 49th campaign of November 2008.

Figure 10 shows a photograph of experimental setup. The liquid flow has been started 1 minute before each parabola and finished in the beginning of the second hypergravity period. All of the liquid supply system components as well as test section are enclosed inside the Experimental Container. It represents the liquid-tight apourum box with two removable opposite walls. After the test section the mixture of apour, gas and liquid moves into the vent system of aircraft. The mixture is evacuated to the atmosphere by vacuum pump.

3. EXPERIMENTAL RESULTS

3.1. On-Ground Experiments

The main goal of the on-ground experiments with rivulet flows was to investigate the geometrical characteristics of the rivulet's profile in a wide range of the flow parameters in the cases of isothermal flow. The test section with partially closed nozzle was used, see Fig. 3. Width of the rivulet and profile of the upper part of the rivulet have been measured at various surface temperatures for vide range of gas and liquid flow rates.

In Fig. 11 the effect of gas flow rate on the width of rivulet is shown. Rivulet width decreases with the gas flow rate growth. The basic interpretation consists of two aspects: 1) the speed of the rivulet at a constant liquid flow rate increases with the gas flow rate. As a result, the width of the rivulet should be reduced; 2) the width of the rivulet reduces due to evaporation. Dry nitrogen and highly volatile fluorinate liquid were used in the experiments.

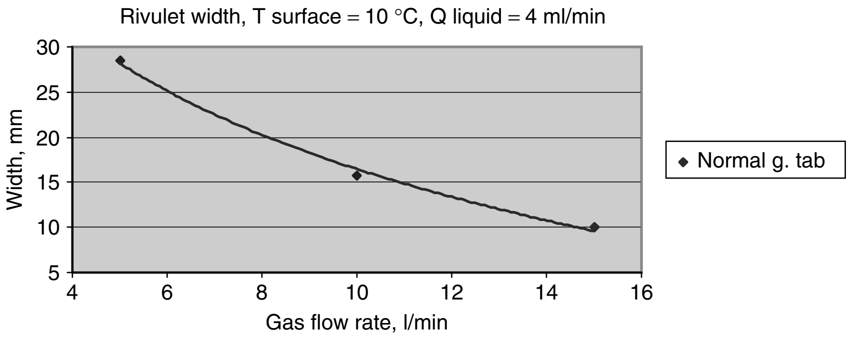

Figure 11. Gas flow rate effect on the width of rivulet.

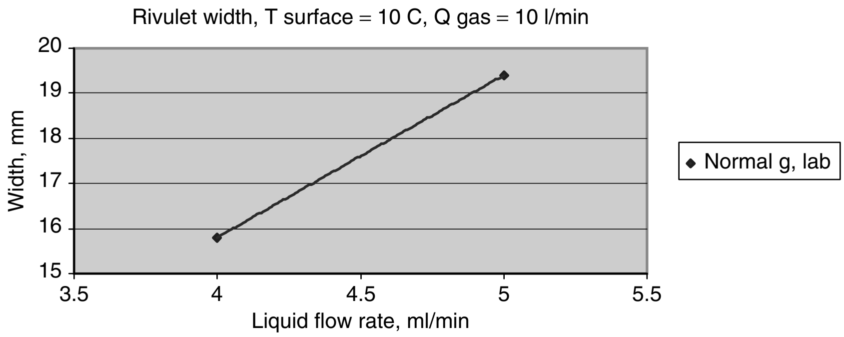

Figure 12. Liquid flow rate effect on the width of rivulet.

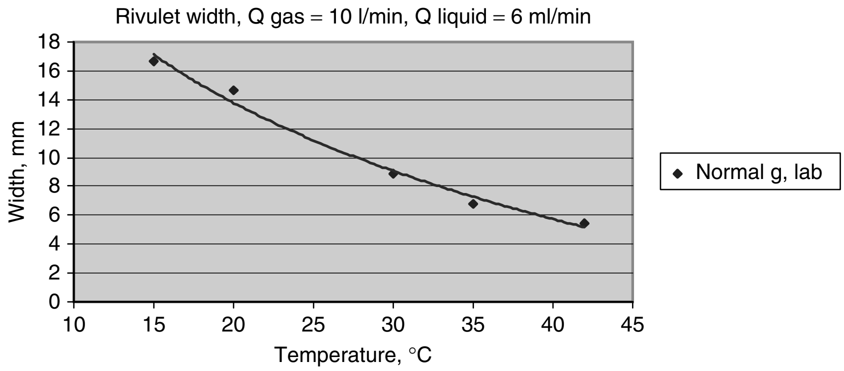

Figure 13. Surface temperature effect on the width of rivulet.

The influence of the liquid flow rate is shown in Fig. 12. Width of the rivulet increases with the liquid flow rate. In the first approximation since the rivulet is flat the shear force on the gas-liquid interface is almost the same for the given gas flow rate (not change in spanwise direction). The velocity of the liquid should be also almost constant and not vary in spanwise direction. Therefore, at a constant gas flow rate the width of the rivulet should increase with increase of the flow rate of the liquid to accommodate more liquid.

The influence of the surface temperature on the rivulet width is shown in Fig. 13. The width of the rivulet reduces with increase of the surface temperature. This trend is caused, most probably, by the evaporation effect.

The 3D profiles of the moving rivulets were measured with the help of the PSS technique during the process of the experiments. Only the upper part of the profiles were considered, where the uncertainty of the optical system did not exceed 1 μm. The example of the measured 3-D profile of the rivulet is presented in Fig. 14. The 2D profiles in different cross-sections of the flow were reconstructed on the base of the measured 3-D profiles as it is shown in Fig. 15. The distance from the nozzle corresponds approximately to 50 mm for the profile 1 and to 60 mm for the profile 2.

3.2. Parabolic Flight Experiments

Validation of the procedures how to organize a gas shear-driven liquid film and rivulet flow under microgravity conditions has been done during several ESA parabolic flights campaigns. The specifics of the parabolic flights environments are: vibrations, short time for experiment, and movement of the axis of the aircraft. It was found in general that the flow dynamics in normal gravity differs significantly from that in Microgravity. The film is wavier under Microgravity conditions. Some preliminary results have been published in [13, 21].

Variations of acceleration during the aircraft manoeuvre and photographs of the rivulet at different levels of gravity are shown in Fig. 16. Schlieren visualization of the crosswise deformations has been made. Rivulet width versus liquid flow rate for constant surface temperature and gas flow rate and for different levels of gravity is shown in Fig. 17. The rivulet width increases with the liquid flow rate and

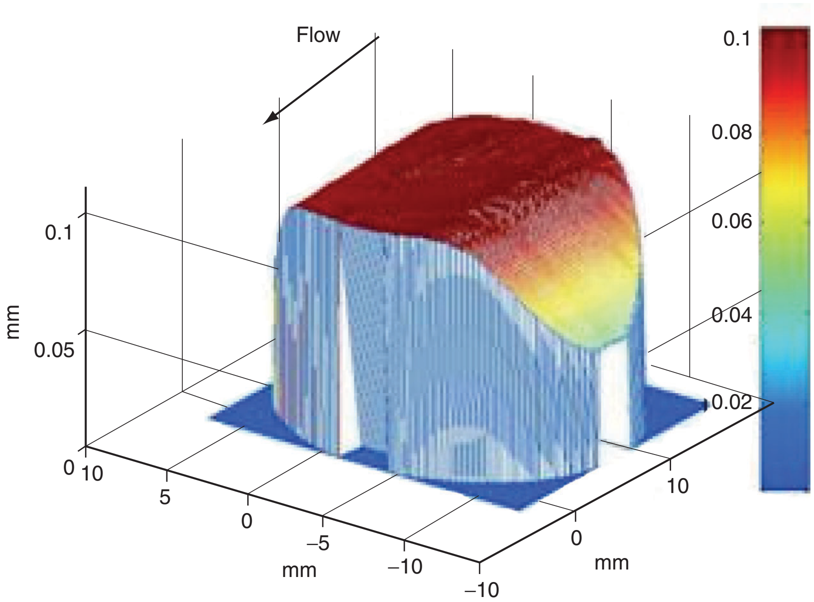

Figure 14. The 3-D profile of the upper part of rivulet: $T_{surface}$ = 10 °C, Q_{gas} = 10 l/min, Q_{liquid} = 4ml/min.

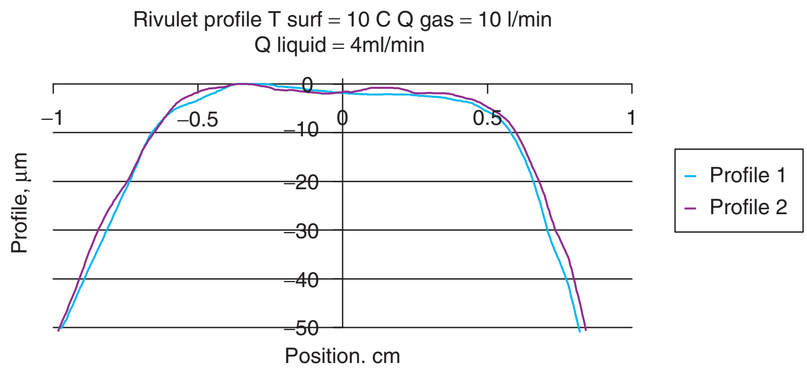

Figure 15. The cross sections of the rivulet flow (reconstructed on the base of the 3-D profile.

the level of gravity. At hyper gravity, the width of the rivulet can exceed twice the width of the rivulet at microgravity.

Rivulet width versus gas flow rate for constant surface temperature and liquid flow rate and for different level of gravity is shown in Fig. 18. The width decreases with the gas flow rate increases. The basic interpretation is the same as in Fig. 11.

Substrate temperature effect on the width of the rivulet is shown in Fig. 19. Results of the measurements are shown at constant gas and liquid flow rates. The width reduces with the surface temperature growth, most probably, due to evaporation. The dependence becomes weaker with the gravity level decreasing, which can be explained by the variation of the surface of the rivulet. The higher is gravity the flatter is the rivulet and, respectively, the bigger its surface and evaporation rate.

Figures 20 and 21 show the 3-D profile of the rivulet measured at the normal gravity (Fig. 20) and 3-D profile of the rivulet measured at microgravity (Fig. 21) under the same conditions. One can see that at microgravity, the surface of the rivulet becomes wavier. Comparison of figures shows that the gravity has a stabilizing effect on the liquid flow as also was obtained in the previous parabolic flight experiments of October 2005 and October 2007 [13, 21].

Figure 22 represents the 2-D profile of the rivulet's cross section at microgravity in comparison with that measured for the same flow parameters at the normal gravity in flight and under on-ground

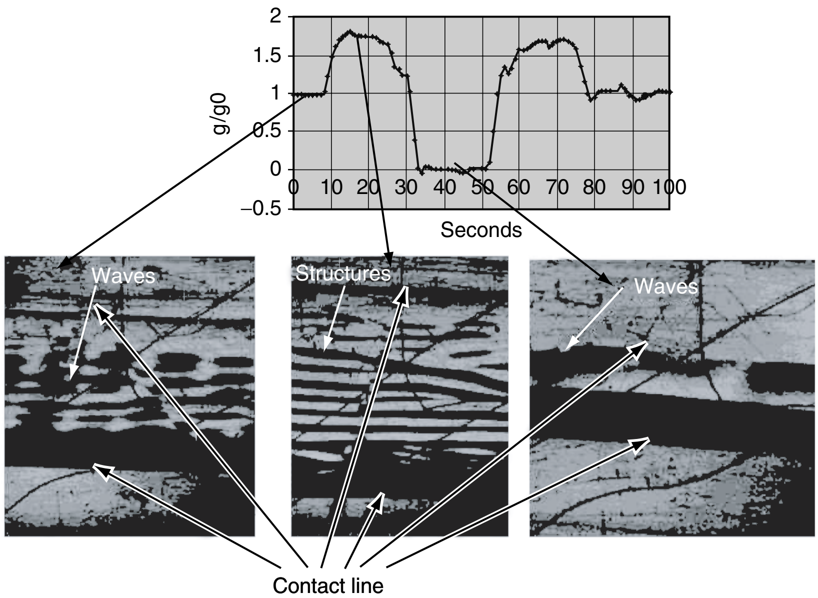

Figure 16. Variations of acceleration during the aircraft maneuver and photographs of the rivulet at different levels of gravity, Qgas = 10 l/min, Qliquid = 7 ml/min, T = 20° C (Schlieren visualization for spanwise deformations).

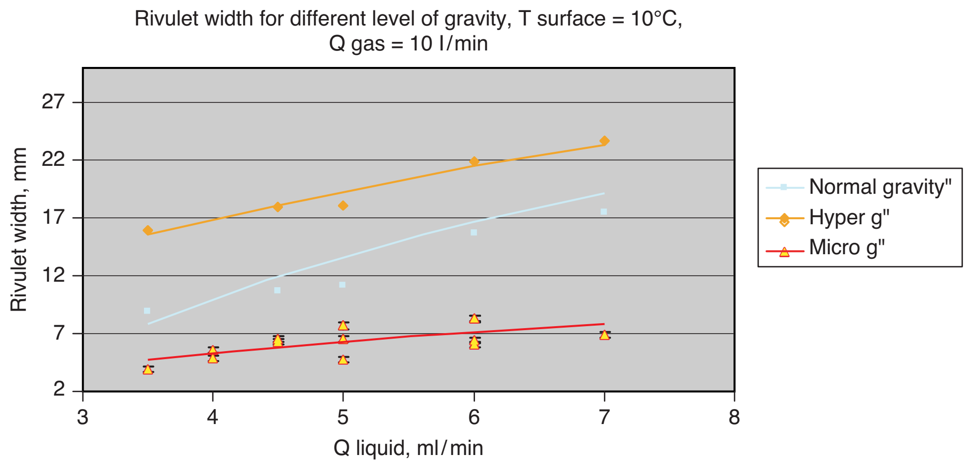

Figure 17. Rivulet width versus liquid flow rate for constant surface temperature and gas flow rate.

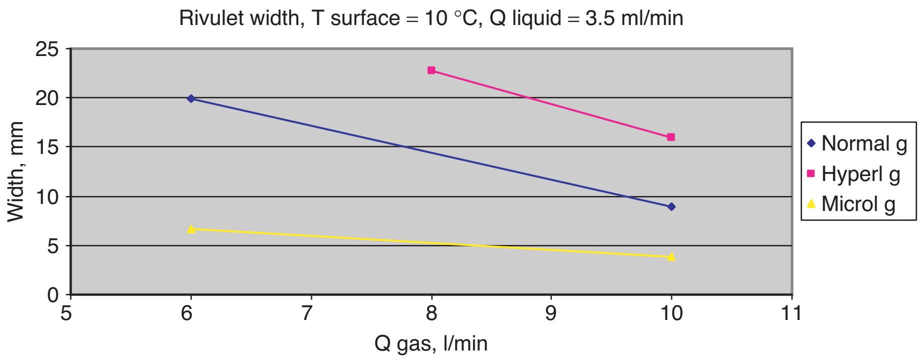

Figure 18. Rivulet width versus gas flow rate for constant surface temperature and liquid flow rate and for different level of gravity.

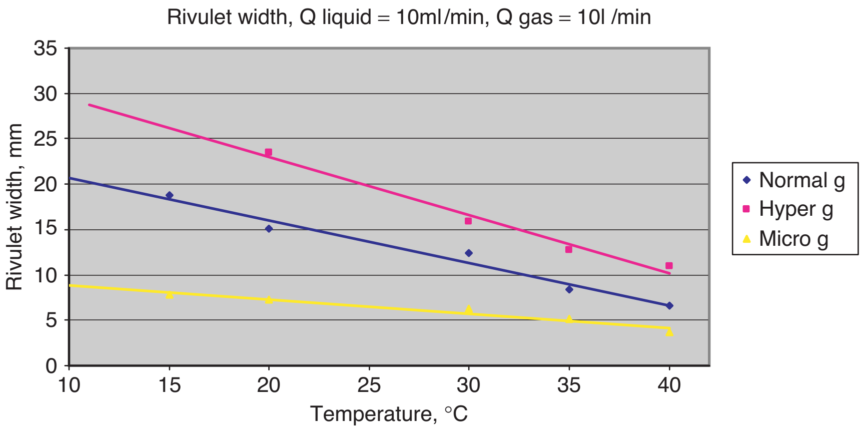

Figure 19. Substrate temperature effect on the width of the rivulet.

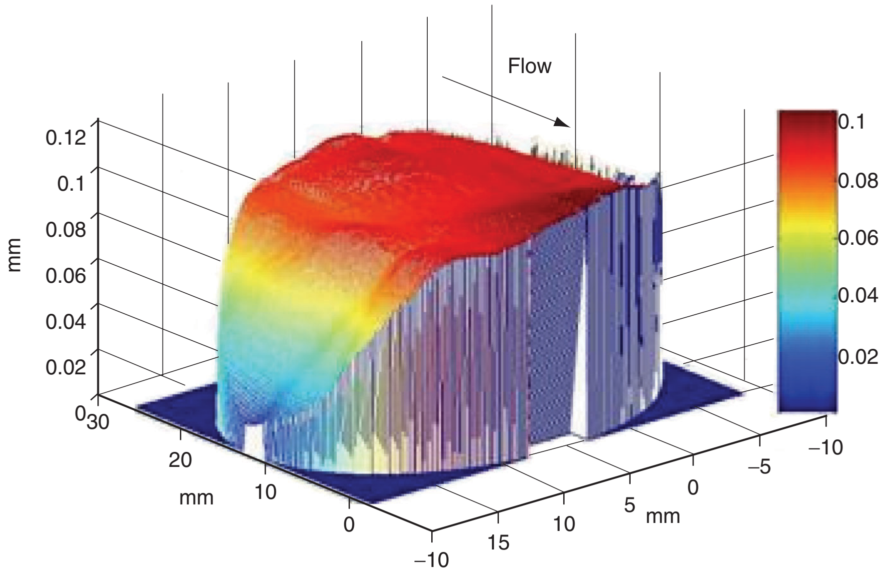

Figure 20. 3-D profile of rivulet at normal gravity.

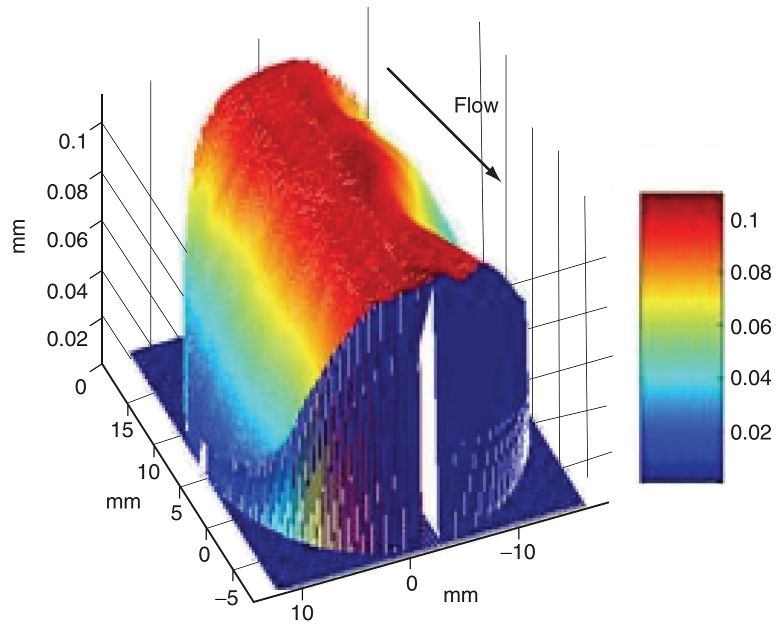

Figure 21. 3-D profile of rivulet at microgravity.

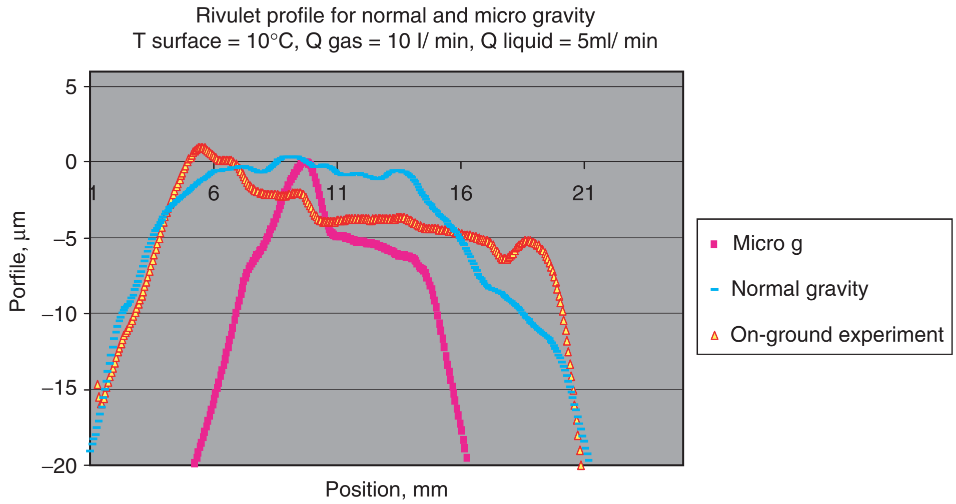

Figure 22. 2-D profiles of the rivulet cross section at different gravity conditions.

conditions. Only the upper parts of the profiles are considered, where the uncertainty of the optical system does not exceed ~ 1 µm. One can see that the profiles obtained at the normal gravity in flight and in the laboratory conditions are very close, while at microgravity the profile is narrower than in normal gravity conditions. It should be noticed that the scales in vertical and horizontal directions are different by three orders of magnitude.

4. MATHEMATICAL MODEL AND COMPUTATIONS

4.1. Mathematical Model for a Shear-Driven Rivulet Flow

We have used a model of the rivulet flow in a horizontal minichannel developed in [19, 20]. The cross section of rivulet is supposed to be invariable. The solutions of the Navier-Stokes equations describe the steady laminar shear-driven rivulet flow. For flattened rivulet we can obtain Poisson equation for velocity. Also, it is known that in the shear-driven rivulet flow the liquid velocity profile is very close to linear and we can define the liquid velocity in flattened rivulet as $v = \tau/\mu \cdot z$ (linear dependence from z). The liquid flow rate in the rivulet cross section Ω can be found as

$$Q = \iint_{\Omega} v dz . \tag{2}$$

The rivulet profile $z = H(y)$ can be received from the solution of the nonlinear equation [19, 20]

$$\frac{H''}{(1+H'^2)^{3/2}} - q^2 H + C_1 = 0, \tag{3}$$

and linearized equation valid in the case of $tan^2\Theta <<1$ and $H'^2<<1$

$$H'' - q^2 H + C_1 = 0 \tag{4}$$

with boundary conditions

$$H(-b) = H(b) = 0, \tag{5}$$

where C_1 is a constant subject to estimation from additional boundary conditions

$$H'(-b) = tan\theta,\ H'(b) = -tan\theta. \tag{6}$$

The exact solution of linear equation (4) is an analytical formula for free surface

$$H(y) = \frac{tan\theta}{q \operatorname{sh} qb}(\operatorname{ch} qb - \operatorname{ch} qy). \tag{7}$$

The analytical formula for the flow rate can be found from (7) and integral (2) in the form:

$$Q = \frac{\tau tan^2\theta}{2\mu q^2 \operatorname{sh}^2 qb}\left(2b\operatorname{ch}^2 qb - \frac{3}{q}\operatorname{ch} qb \cdot \operatorname{sh} qb + b\right). \tag{8}$$

Where $\tau = (6\mu_g Q_g / d^2 l)$. From analytical formula (8), which connected the main rivulet parameters, the following equation can be derived:

$$3\frac{\mu_g}{\mu}\cdot\frac{Q_g}{Q_l}\cdot\frac{1}{d^2 l} tg^2\theta \cdot \frac{1}{\frac{\rho g}{\sigma}\cdot sh^2\left(\sqrt{\frac{\rho g}{\sigma}}b\right)}\cdot \cdot\left(2bch^2\left(\sqrt{\frac{\rho g}{\sigma}}b\right) - \frac{3}{\sqrt{\frac{\rho g}{\sigma}}} ch\left(\sqrt{\frac{\rho g}{\sigma}}b\right) sh\left(\sqrt{\frac{\rho g}{\sigma}}b\right) + b\right) = 1. \tag{9}$$

Then at $g \to 0$ we can obtain the equation:

$$\frac{4}{5}\cdot\frac{\mu_g}{\mu}\cdot\left(\frac{Q_g}{Q_l}\right)\cdot\frac{1}{d^2 l}\cdot tg^2\theta\cdot\left(\frac{1}{7}\frac{\rho g}{\sigma}\cdot b^5 - b^3\right) + 1 = 0. \tag{10}$$

In a special case of $g = 0$ the following analytical formula for rivulet semi-width may be obtained:

$$b = \sqrt[3]{\frac{5}{4}\cdot\frac{\mu}{\mu_g}\cdot d^2 l \cdot tg^{-2/3}\theta\cdot(Q_l/Q_g)^{1/3}}. \tag{11}$$

As it was shown in [19] in a special case of the large values of gravity function $b = b(g)$ has an inclined asymptote:

$$b = \frac{Q\rho\mu}{\tau\sigma \operatorname{tg}^2\theta} g + \delta. \tag{12}$$

Formulas (10) and (11) show that, in this particular case of negligible gravity effect, the width of the rivulet depends on geometrical parameters of the minichannel (d and l), contact angle Θ, the ratio of liquid and gas dynamic viscosity (μ/μ_g) and the ratio of liquid and gas flow rates (Q_l/Q_g).

The geometrical parameters exist in the formulas because at constant gas and liquid flow rates they define the tangential shear-stress on the gas-liquid interface. The results of the numerical solution of the equation (10) on the semiwidth of rivulet b for different values of contact angle θ are shown in Fig. 23. Properties of liquid correspond to FC-72 and properties of gas correspond to Nitrogen. The cross-section of the minichannel is 1470 μm × 40 mm. The width of the rivulet decreases with the gas-liquid flow rates ratio increasing. Increasing of the value of contact angle causes decreases of the width of the rivulet.

4.2. Rivulet Flow in Micro-Channels

The results of numerical calculations of the liquid and gas velocity fields and other rivulet parameters (width, profiles) for different levels of the gravity were presented in [22]. It was found that a thin liquid rivulet deforms significantly the velocity field in the gas phase. For the regimes described in [22] it was shown that the surface of the rivulet, flowing in the horizontal minichannel under the action of the co-current gas flow and gravity, becomes almost flat at gravity exceeding one third of the earth gravity level.

Figure 24 presents the velocity field in cross-section of minichannel with the height of 1.4 mm and the width of 40 mm. It should be noticed that the scales in vertical and horizontal directions are different by one order of magnitude. The field of rivulet flow is sharply defined, as the rate of liquid

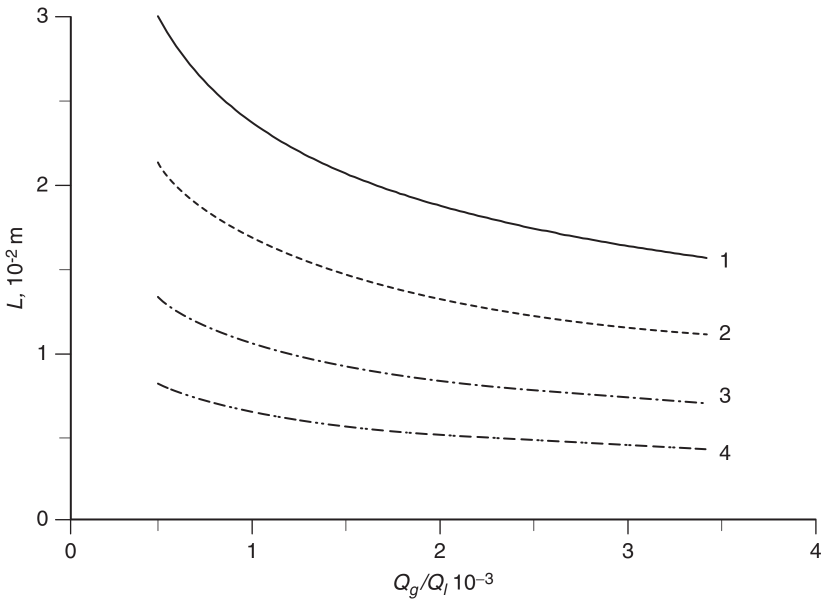

Figure 23. Changing the width of rivulet with increasing the ratio of gas and liquid flow rates for various values of contact angle θ (1- $\theta = 3°$, 2- $\theta = 5°$, 3- $\theta = 10°$, 4- $\theta = 20°$), $g \to 0$.

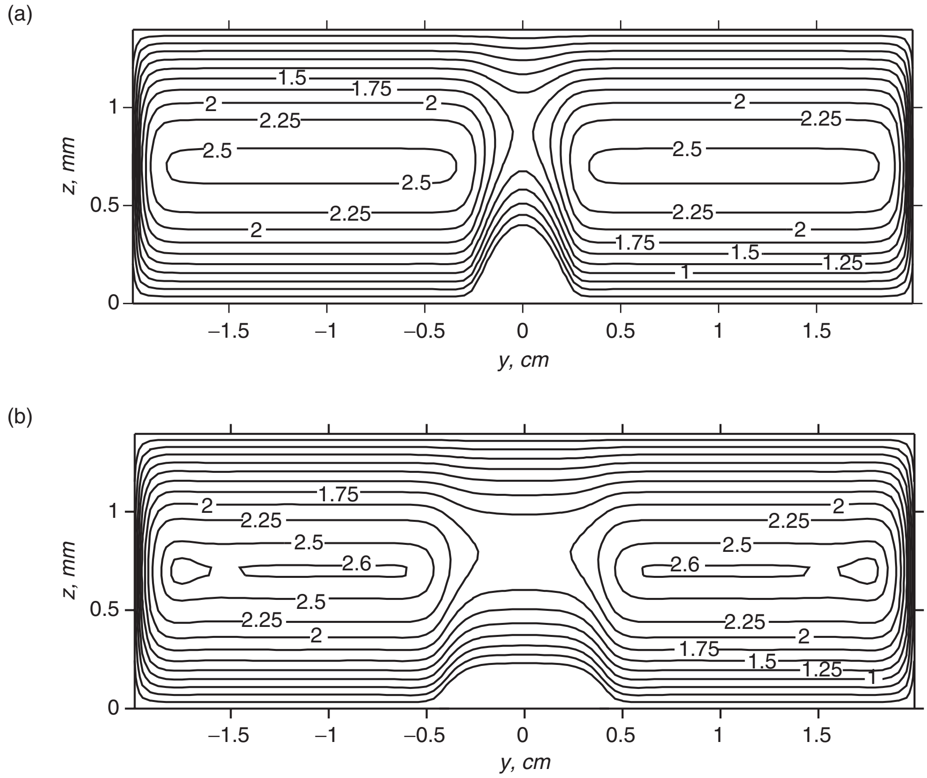

Figure 24. Velocity field in cross-section of mini-channel (m/s). (a) – microgravity ($g = 0.0001 g_0$), (b) – hyper gravity ($g = 1.5 g_0$); $\theta = 16°$, $Q_l = 0.180E\text{-}07$ м^3/с, $Q_g = 0.87500E\text{-}04$ м^3/с, Rel = 1.1, Reg = 154

is two orders of magnitude smaller than the rate in the gas. Figure 24a shows the velocity field in cross-section of minichannel in liquid and gas phases in microgravity conditions (g = 0.001 m/s^2). Figure 24b shows the velocity fields for the same flow parameters but in hyper gravity conditions (g = 14.7 m/s^2). There is a significant effect of gravity on the shape of the rivulet. The rivulet in

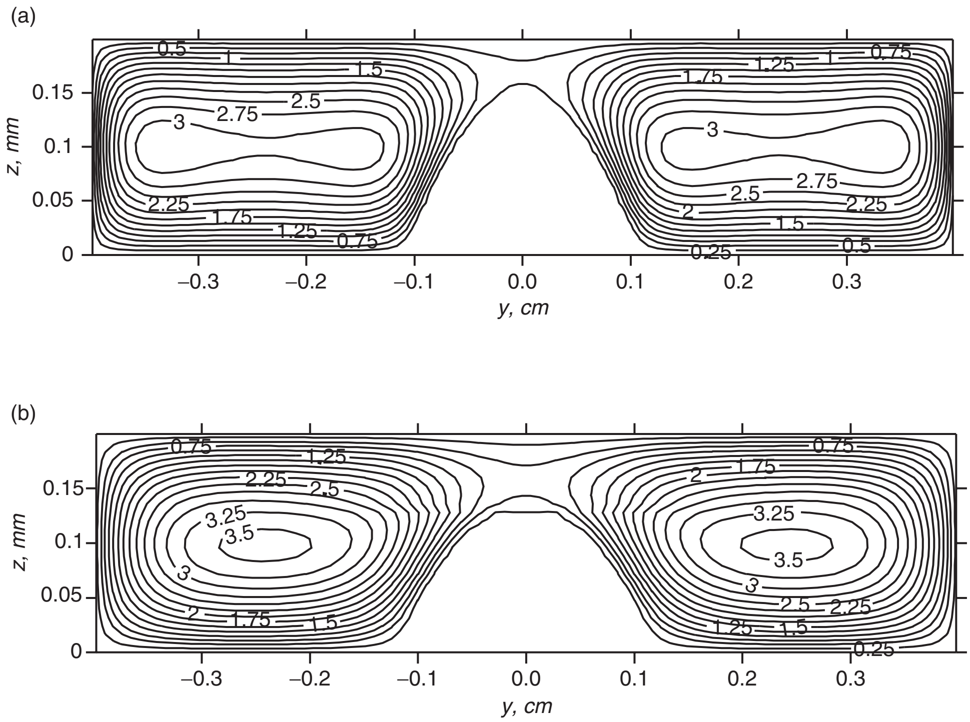

Figure 25. Velocity field in cross-section of micro-channel (m/s). (a) – microgravity ($g = 0.0001g_0$), (b) – hyper gravity ($g = 1.5g_0$); $\theta = 16°$, $Q_l = 0.18E\text{-}07$ м³/с, $Q_g = 0.25E\text{-}05$ м³/с, $Re_l = 5.4$, $Re_g = 22$

minichannel is flattened with gravity increasing and the width of the rivulet increases by the factor 1.6 with gravity changing.

From the results of our calculations we can conclude that the presence of even microscale rivulet flow on the bottom wall of the minichannel modifies significantly the velocity field in the gas phase. In conditions of the significant gravity, there is a flat gas-liquid interfacial surface and the plane-parallel rivulet flow with a constant tangential stress at the interface take place.

Figure 25 presents the velocity field in cross-section of microchannel with the height of 0.2 mm and width of 8 mm. Figure 25a shows the velocity fields at microgravity conditions ($g = 0.001$ m/s^2) and Fig. 25b shows the velocity fields for the same flow parameters but in hyper gravity conditions (g = 14.7 m/s^2). The dimensions of channels in Fig. 24 and Fig. 25 are different, but for the comparability of conditions the liquid flow rates and the gas superficial velocities are the same in the both cases. We can see that gravity has almost no effect on the shape of the rivulet in the case of the microchannel. In other words, it was found that in microchannels, in contrast to minichannels, there is no flattening of the rivulet surface with the increasing of the gravity.

Thus, with the decreasing of the height of the channel, the force balance in the rivulet is changing and the influence of the gravity on the rivulet flowing reduces. Perhaps, the main reason for this effect is that the absolute value of the average velocity of the liquid in microchannel increase by a factor 5–10 due to a significant shear stress on the gas-liquid interface increase. Also an uneven distribution of the shear stress on the gas-liquid interface can be important. It is important to notice again that the gas superficial velocity and the liquid flow rate remain the same for microchannel and minichannel.

4.3. Mathematical Model for a Gravity-Driven Rivulet Flow

For the case of the gravitational rivulet flowing down an inclined surface we have dependence, similar to (8), [20]:

$$Q = \frac{\rho g \sin\beta \,\mathrm{tg}^3\theta}{9\mu q^4}(15(qb)\,\mathrm{cth}^3(qb) - 15\,\mathrm{cth}^2(qb) - 9(qb)\,\mathrm{cth}(qb) + 4). \tag{13}$$

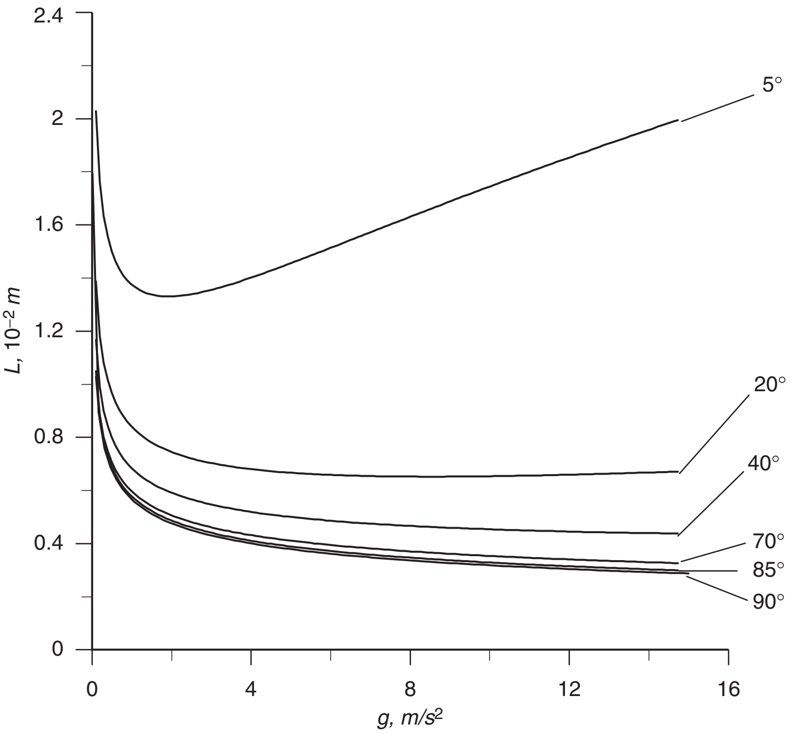

Figure 26. Changing the width of rivulet $L = 2b$ with increasing of gravity for different inclination angles of the minichannel $\beta = 5°, 20°, 40°, 70°, 85°, 90°$; $\theta = 16°$, $Re_l = 7.6$ [20].

At $g \to 0$ it was obtained that the rivulet width has power law dependence on gravity:

$$b(g) = \sqrt[4]{\frac{105\mu Q}{4\rho \sin\beta \,\mathrm{tg}^3\theta}} \cdot \frac{1}{\sqrt[4]{g}} + o\left(\frac{1}{\sqrt[4]{g}}\right). \tag{14}$$

Proportionality $Q \sim 4b^4/105$ is similar to [28]. For the case of the large values of gravity function we have obtained [20] the expression:

$$b(g) = \left(\frac{\cos\beta}{\sigma}\right)^{3/2} \frac{3\mu\sqrt{\rho}}{2\sin\beta \,\mathrm{tg}^3\theta} Q\sqrt{g} + o\left(\sqrt{g}\right) \tag{15}$$

The change of the functional dependence $b = b(g)$ from (14), $b \sim g^{-1/4}$, to (15)), $b \sim g^{1/2}$, takes a place with gravity increasing. Figure 26 shows that this change of functional dependence is most essential at small angles of inclination of the surface. The numerical calculations were carried out for minichannel with cross-section 1400 μm × 40 mm for the liquid FC-72.

The critical point g of change of the functional dependence from (14) to (15) depends on the angle of inclination of the channel and the contact angle. The presence of inclination of the surface makes the width of the rivulet less sensitive to the gravity.

5. COMPARISON OF THEORETICAL AND EXPERIMENTAL RESULTS

5.1. Comparison with Theory for On-Ground Experiments

Comparison of rivulet profile for on-ground experiments with theoretical model is shown in Fig. 27 and Fig. 28. Different series of experiment for the same parameters mean different measurements. Profile has been measured in several parts of rivulet for the same series. A satisfactory qualitative and quantitative agreement of experimental and theoretical results is seen.

The best approximation corresponds to the contact angle $\theta = 13°$. It is visible that the deviation of experimental and theoretical results is much higher than 1 μm (uncertainty of the optical measurement system) especially for Fig. 28. There can be several reasons: 1) dynamic contact angle

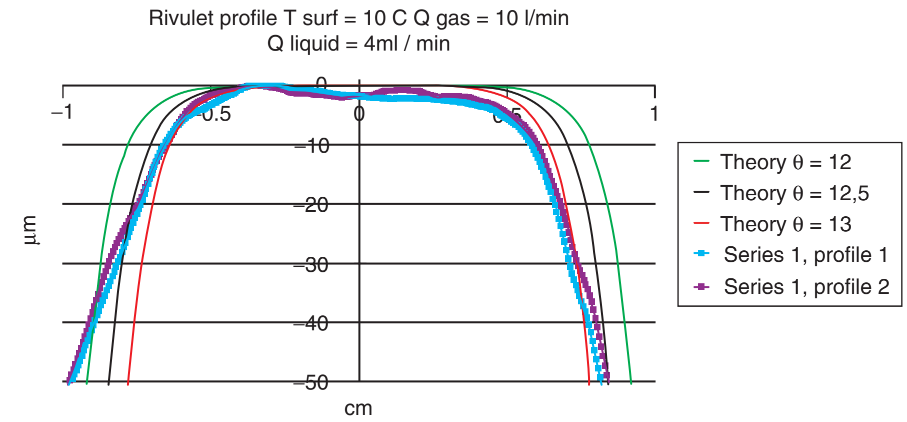

Figure 27. Comparison of experimental and theoretical results in the on-ground conditions; distance from the nozzle for a profile 1 is equal to 50 mm and for the profile 2 is equal to 60 mm.

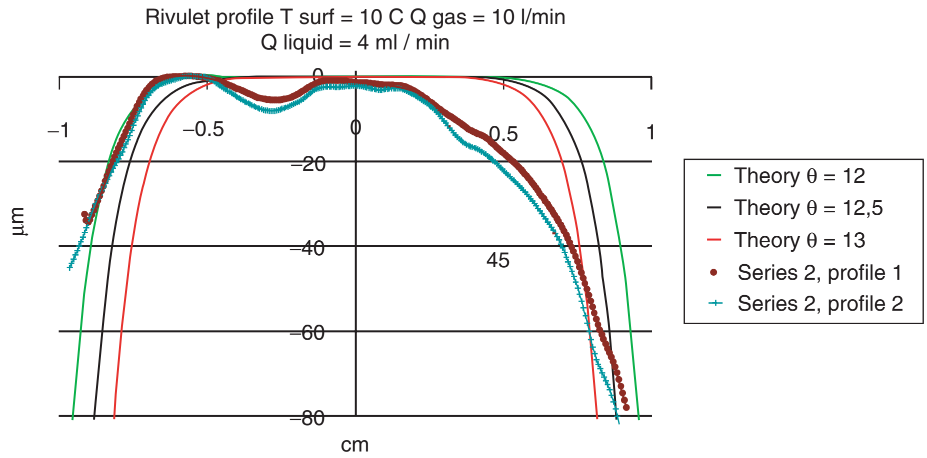

Figure 28. Comparison of experimental and theoretical results in the on-ground conditions; distance from the nozzle for a profile 1 is equal to 50 mm and for the profile 2 is equal to 60 mm.

that is not included in the theoretical model; 2) neglecting of evaporation effect that is also not taken into account in the theoretical model; 3) waves in the rivulet that can bring a bigger measurement uncertainty.

5.2. Comparison with Theory for Parabolic Flight Experiments

Figure 29 shows the comparison of numerical calculations for the ratio of gas and liquid flow rates equal to 2000 with the experimental data obtained during parabolic flights in the framework of the 47th and 49th ESA campaigns. Channel parameters correspond to the test section TS-1 in [21]. The channel high $d = 1470$ μm, width $l = 40$ mm, liquid FC-72, gas Nitrogen.

Numerical calculations have been done for the contact angle values equal to $\theta = 10°$, 15° and 20°. One can see that the best correspondence of experimental and theoretical results in the parabolic flights conditions take place at the contact angle $\theta = 15°$. Unfortunately, the real contact angle in this experiment was not measured. It can be estimated using an empirical formula [29] (for details see also 21).

Figure 29 shows the comparison of numerical calculations and experimental results for the one ratio of gas and liquid flow rates that is equal to 2000. Numerical calculations of the width of rivulet for different levels of gravity and the ratios of gas and liquid flow rates are shown in Fig. 30. The channel size, gas and liquid are similar to Fig. 29. The value of a temperature difference between the hot substrate and a cold rivulet has been estimated as 6°C. The contact angle corresponding to this temperature difference has been calculated as $\theta = 22.56°$ according to empirical formula [29]. Figure 30

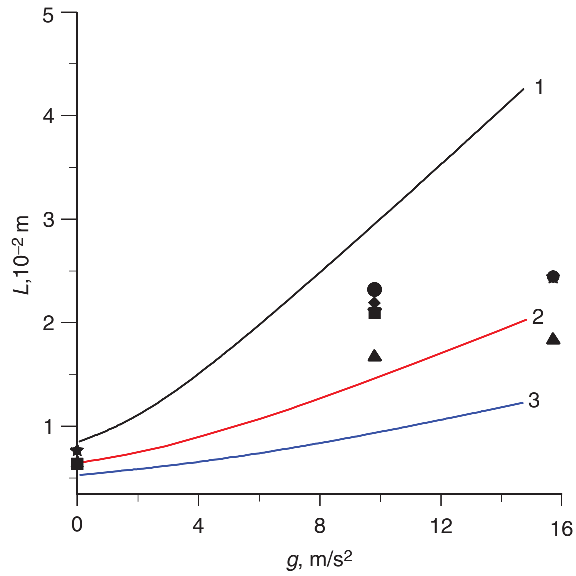

Figure 29. Variation of the rivulet width with increasing of gravity for the ratio of the liquid-gas flow rates $Q_g/1000Q_l = 2$, θ: 1 – 10º, 2- 15°, 3- 20º; • - $Q_g = 6$ l/min, $Q_l = 3$ ml/min, ▲ - $Q_g = 4$ l/min, $Q_l = 2$ ml/min, ■ - $Q_g = 8$ l/min, $Q_l = 4$ ml/min, ◆ - $Q_g = 10$ l/min, $Q_l = 5$ ml/min, ★ - $Q_g = 10$ l/min, $Q_l = 5$ ml/min.

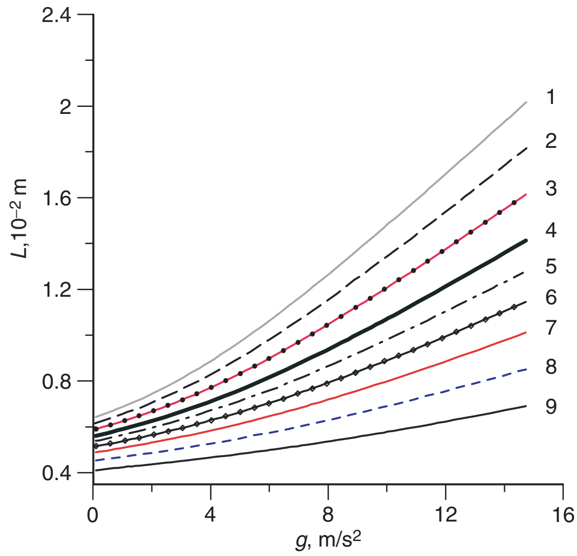

Figure 30. Rivulet width versus gravity for several ratios of the liquid-gas flow rates $Q_g/1000Q_l$: 1 – 0.88, 2 – 1, 3 – 1.14, 4 – 1.33, 5 – 1.5, 6 – 1.71, 7 - 2, 8 – 2.5, 9 – 3.33, $\theta = 22.56°$.

shows that for the smallest ratio of gas flow rate to liquid flow rate the dependence of rivulet widths on gravity is a strongest. With decreasing of ratio of gas flow rate to liquid flow rate the dependence of rivulet widths on gravity became weaker.

6. CONCLUSIONS

The paper provides an overview of the recent progress that has been achieved in the experimental and theoretical investigations of rivulet flows in micro- and mini- channels. Experimental results for the rivulet flowing in the different conditions were obtained in several parabolic flights campaigns of the European Space Agency as well as in the standard laboratory environment.

It was found theoretically and numerically that the main parameters determining the shape of the rivulet are the thermal contact angle, the level of gravity, the angle of inclination of the substrate to the horizon and the value of the shear stress on the gas-liquid interface. For the gravity-driven rivulet flow regime it was shown that the presence of significant inclination of the surface makes the width of the rivulet less sensitive to the gravity.

The experimental results and numerical calculations predict that with the gas flow rate increasing, the width of rivulet decreases. Also, it was shown that with gas-liquid flow rates ratio increasing the width of rivulet decreases and that for smaller flow rates ratios the rivulet widths is greater. It was demonstrated that with the decreasing of the height of the channel, the influence of the gravity on the rivulet flowing reduces.

ACKNOWLEDGEMENTS

The authors gratefully acknowledge support of this work by SAFIR PRODEX Programme (Belgium) and ESA in the framework of ESA Parabolic Flight Campaigns as well as by the Russian Foundation for Basic Research (project # 05–08–65426) and by Siberian Branch of Russian Academy of Sciences on integrated project # 64. The authors are thankful to Andrey Glushchuk and Sergey Chikov for their contribution in the experimental investigations.

REFERENCES

[1] Towell G.D., Rothfeld L.B., *Hydrodynamics of rivulet flow*, AIChE Journal, Vol.12, No.5, 1966, pp. 972–980.

[2] Allen R.F., Biggin C.M., Longitudinal flow of a lenticular liquid filament down an inclined plane, *The Physics of Fluids*, Vol.17, No.2, 1974, pp. 287–291.

[3] Bentwich M., Glasser D., Kern J., Williams D., *Analysis of rectilinear rivulet flow*, AIChE Journal, Vol.22, No.4, 1976, pp. 772–779.

[4] Schmuki P., Laso M., On the stability of rivulet flow, *J.Fluid Mech.*, Vol.215, 1990, pp.125–143.

[5] S. V. Alekseenko, P. I. Geshev, and P. A. Kuibin, *Free-Boundary Fluid Flowon an Inclined Cylinder*, Doklady Physics, Vol. 42, No. 5, 1997, pp. 269–272.

[6] Perazzo C.A., Gratton J., Navier-Stokes solutions for parallel flow in rivulets on an inclined plane, *J.Fluid Mech.*, Vol. 507, 2004, pp. 367–379.

[7] Alekseenko S.V., Markovich D.M., Shtork S.I., Wave flow of rivulets on the outer surface of an inclined cylinder, *Phys.Fluids*, Vol.8, 1996, pp. 3288–3299.

[8] Alekseenko S.V., Antipin V.A., Bobylev A.V., Markovich D.M., Application of PIV to velocity measurements in a liquid film flowing down an inclined cylinder, *Exp.Fluids*, Vol.43, 2007, pp. 197–207.

[9] Alekseenko S. V., Markovich D. M., Nakoryakov V. E. and Shtork S. I., Rivulet flow of liquid on the outer surface of an inclined cylinder, *Journal of Applied Mechanics and Technical Physics*, Vol. 38, No. 4, 1997, pp. 649–653.

[10] Alekseenko S.V., Bobylev A.V., Kharlamov S.M., Markovich D.M., *Frequency susceptibility of rivulets flowing down vertical plate*, *14th Int. Symp on Applications of Laser Techniques to Fluid Mechanics*, Lisbon, Portugal, 07–10 July, 2008.

[11] Gambaryan-Roisman T., Stephan P., Flow and Stability of rivulets on heated surfaces with topography, *Journal of Heat Transfer*, Vol.131, 2009, pp. 033101–1–033101–6.

[12] Kabov O.A., Formation of regular structures in a falling liquid film upon local heating, *Thermophysics and Aeromechanics*, Vol. 5, No. 1, 1998, pp. 547–551.

[13] Kabov O., Cooling of Microelectronics by Thin Liquid Films, Keynote lecture, *Proc. Int. Workshop on "Wave Dynamics and Stability of Thin Film Flow Systems"*, September 1–4, Chennai, India, Narosa Publishing House, 2006, pp. 279–311.

[14] Kabov O.A. and Chinnov E.A., Heat Transfer From a Local Heat Source to a Subcooled Falling Liquid Film Evaporating in a Vapor-Gas Medium, *Russian Journal Engineering Thermophysics*, Vol. 7, No. 1–2, 1997, pp. 1–34.

[15] Chinnov E.A. and Kabov O.A. Jet Formation in Gravitational Flow of a Heated Wavy Liquid Film. *Journal of Applied Mechanics and Technical Physics*, Vol. 44, No. 5, 2003, pp. 708–715.

[16] Pavlenko A.N. and Lel V.V., Heat Transfer and Crisis Phenomena in Falling Films of Cryogenic Liquid , *Russian Journal of Engineering Thermophysics,* Vol. 7, No. 3–4, 1997, pp. 177–210.

[17] Pavlenko A.N., Lel V.V., Serov A.F., Nazarov A.D., Matsekh A.D., The growth of wave amplitude and heat transfer in falling intensively evaporating liquid films, *Russian Journal of Engineering Thermophysics*, Vol. 11, No. 1, 2002, pp. 7–43.

[18] Myers T.G., Liang H.X., Wetton B., The stability and flow of a rivulet driven by interfacial shear and gravity, *International Journal of Non-Linear Mechanics*, Vol.39, 2004, pp. 1239–1249.

[19] Bartashevich M.V., Kuznetsov V.V. and Kabov O.A., *Mathematical modeling of rivulet flow driven by variable gravity and gas flow in a minichannel*, Proceedings of the 6th Int. Conf. on Nanochannels, Microchannels and Minichannels, ICNMM2008, June 23–25, 2008, Darmstadt, Germany, pp. 1–8.

[20] Bartashevich M.V., Kuznetsov V.V., Kabov O.A., The rivulet flowing in inclined minichannel with co-current gas flow in conditions of variable gravity, *Sib. Zh. Ind. Mat.,* Vol.12, No.2 (38), 2009, pp. 3–16 (in Russian).

[21] Kabov O.A., Bartashevich M.V., Glushchuk A., Cheverda V., *The effect of variable gravity and shear stress on the flattened rivulet dynamics in a minichannel*, 1st European Conference on Microfluidics - Microfluidics 2008 - Bologna, December 10–12, 2008, paper μFLU08–232.

[22] Bartashevich M.V., Kuznetsov V.V., Kabov O.A., Dynamics of the restricted liquid film in co-current gas flow in microchannel, *Fluid Dynamics* (in press).

[23] Joannes L., Beghuin D., Ligot R., Farinotti S., Dupont O., *High resolution shape measurements with Phase-Shifting Schlieren (PSS)*, Proc. SPIE (Optical metrology in Production), Bellingham, WA, 5457, 2004, pp. 377–385.

[24] Scheid B., Kabov O. A., Minetti C., Colinet P., Legros J.C., *Measurement of free surface deformation by reflectance-schlieren method*, 3rd European Thermal Science Conference, Sept. 10–13, 2000, Heidelberg, Germany.

[25] Elsinga G.E., van Oudheusden B.W., Scarano F., Watt D.W., Assessment and application of quantitative schlieren methods: Calibrated color schlieren and background oriented schlieren, *Experiments in Fluids*, Vol.36 , 2004, pp. 309–325.

[26] Celata G. P., Colin C., Colinet P., Di Marco P., Gambaryan-Roisman T., Kabov O., Kyriopoulos O., Stephan P., Tadrist L., Tropea C., Bubbles, drops, films: transferring heat in space, *Europhysics News*, 2008, Vol. 39, No. 4, p. 23–25.

[27] Pletser V., Pacros A. and Minster O., International Heat and Mass Transfer Experiments on the 48^{th} ESA Parabolic Flight Campaign of March 2008, *Microgravity sci. technol.*, 2008, Vol. 20, pp. 177–182.

[28] Wilson S.K., Duffy B.R., Unidirectional flow of a thin rivulet on a vertical substrate subject to a prescribed uniform shear stress at its free surface, *Physics of Fluids*, 2005, Vol. 17, p. 108105.

[29] Gerstmann J., Dreyer M.E., The dynamic contact angle in the presence of a non-isothermal boundary condition, *Microgravity sci. technol.*, 2007, Vol. 19, pp. 96–99.